



Li, Q., Xie, B., Zhang, Y., Ma, J., & Yuan, C. (2024). A General Analytical Model of Single-Layer Common-Mode Chokes. *IEEE Transactions on Power Electronics*, 39(6), 6591-6596. Advance online publication. <https://doi.org/10.1109/TPEL.2024.3372297>

Peer reviewed version

License (if available):
CC BY

Link to published version (if available):
[10.1109/TPEL.2024.3372297](https://doi.org/10.1109/TPEL.2024.3372297)

[Link to publication record in Explore Bristol Research](#)
PDF-document

This is the accepted author manuscript (AAM) of the article which has been made Open Access under the University of Bristol's Scholarly Works Policy. The final published version (Version of Record) can be found on the publisher's website. The copyright of any third-party content, such as images, remains with the copyright holder.

University of Bristol - Explore Bristol Research

General rights

This document is made available in accordance with publisher policies. Please cite only the published version using the reference above. Full terms of use are available: <http://www.bristol.ac.uk/red/research-policy/pure/user-guides/ebr-terms/>

A General Analytical Model of Single-Layer Common-Mode Chokes

Qiao Li, Biyan Xie, Yechi Zhang, Jun Ma, and Chao Yuan

Abstract—To accurately model common-mode (CM) chokes is crucial for ensuring the design and optimization of EMI filters. This paper identifies the limitations of the commonly employed analytical model, which results in significant margin errors when applied to CM chokes. It proposes a comprehensive and more precise analytical model that addresses these errors by considering the influence of time-varying electromagnetic fields and the geometric characteristics of CM chokes. Furthermore, this paper provides a detailed explanation of the physical significance behind the proposed model. Both methods are compared, and the suggested approach is validated through simulations and experiments in four distinct scenarios.

Index Terms—CM chokes, electromagnetic interference (EMI), circuit model, electromagnetic analysis.

I. INTRODUCTION

NOWADAYS, trends in designing power electronic devices for lightweight and compact size have led to higher switching frequencies, necessitating stricter compliance with EMI standards [1]. Operating at high frequencies (HF), common-mode (CM) chokes exhibit substantial deviations from the ideal model due to parasitic capacitance related to windings and magnetic cores, leakage inductances, relative permittivity, and permeability of the core. These factors significantly elevate the EMI levels [2-3]. Therefore, accurately modeling CM chokes is essential to optimize EMI filters effectively and enable devices to meet EMI standards without increasing their weight and size.

Existing models for HF CM chokes can be broadly categorized into two main types: behavioral and physical models [4-5]. Among physical modeling methods, the finite element method (FEM) offers high accuracy but demands substantial computational resources [6-7]. Consequently, analytical methods are more promising. The most renowned and highly cited analytical model for CM chokes was developed by Marinko et al. [8]. This model incorporates parameters related to individual winding turns, considers magnetic core material properties, and accounts for mutual coupling among turns and the core. It offers significant design advantages by directly calculating parameters based on geometry. However, the accuracy of the impedance curve decreases when dealing with CM chokes having a small number of turns, which raises concerns due to the increasing significance of such chokes in power electronic devices with higher switching frequencies and lower inductance requirements.

In HF operation, parasitic capacitance plays a pivotal role in the characteristics of CM chokes. Consequently, numerous studies have been conducted to calculate and model parasitic capacitance [9-10]. In a study [3], the calculated capacitance consistently fell short of the measured capacitance when the number of turns was small. The discrepancy, attributed to time-

varying electromagnetic fields inside the core, was extensively discussed in [12]. In summary, accounting for the effects of time-varying electromagnetic fields is crucial when modeling CM chokes.

The remaining sections of this paper are organized as follows: In Section II, the analytical model of CM chokes is introduced in detail. Based on the analysis presented above, in Section III, verification and discussion are conducted among the traditional model, the proposed general model, FEM results, and experimental data. Finally, in Section IV, the paper is concluded.

II. ANALYTICAL MODELING

A. Electromagnetic Behaviour of CM Chokes and Derivation of HF Circuit Model

Fig. 1 illustrates the key geometric parameters of a toroidal CM choke. In this paper, considering the actual geometric structure, the real magnetic core chamfers have been taken into consideration. In the subsequent sections, an enhanced equivalent circuit for modeling CM chokes will be presented, the physical significance of parameters in the proposed circuit model will be discussed, and the calculations for inductance, space capacitance correction, and core capacitance will be explored.

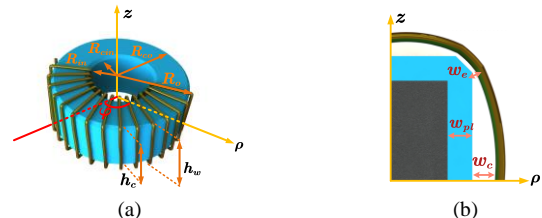


Fig. 1. Geometry and cross section of a toroidal CM choke. R_o and R_{co} are the outer radius of CM choke. R_{in} and R_{cin} is inner radius of CM choke. w_c is maximum distance between turn and core.

For a CM choke, the primary concern lies in its inductive performance, as illustrated in Fig. 2, representing the magnetic field energy within it. However, in high-frequency (HF) scenarios, the presence of displacement currents leads to the existence of electric field energy between turns and between turns and the core. This corresponds to the turn-to-turn capacitance (C_{tt}) and the turn-to-core capacitance (C_{tc}), respectively. Furthermore, due to the time-varying electromagnetic field, a time-varying electric field emerges inside the core, which equivalently corresponds to the core capacitance (C_c). Several studies have addressed the presence of C_c [3], [12]. However, in [8], analytical modeling techniques for CM chokes neglect the existence of C_c , rendering them suitable only for a large number of turns. When dealing with fewer turns, the accuracy of the modeling significantly

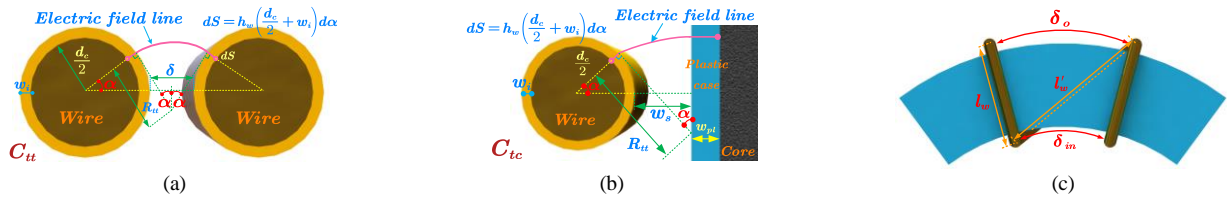


Fig. 3. The geometry between turns, turns and core of a toroidal CM choke. d_c represents the radius of the conductor, w_i stands for the thickness of wire insulation. w_{pi} represents the thickness of core insulation. ϵ_{pi} denotes the relative permittivity of the core insulation. ϵ_a denotes the relative permittivity of air. ϵ_i signifies the relative permittivity of the wire insulation. w_{pi} represents the thickness of core insulation, and ϵ_{pi} denotes the relative permittivity of the core insulation. l_w is winding length parallel to choke.

diminishes. Additionally, all capacitance derivations are based on simplified geometry, resulting in reduced accuracy. In [12], C_c has been discussed, and its relationship with the number of turns has been explored, but no consideration has been given to how C_c should be incorporated into the circuit model and its relationship with different materials. Therefore, a more comprehensive circuit model is developed here, and a detailed discussion on whether C_c should be disregarded for different materials is presented in Section III. Furthermore, the physical implications of constructing circuit models will be thoroughly explored.

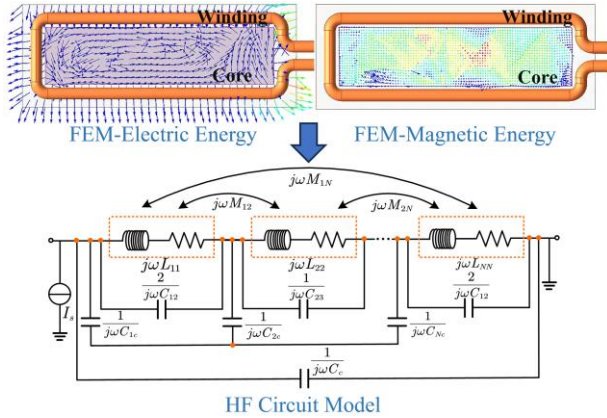


Fig. 2. Proposed equivalent circuit model.

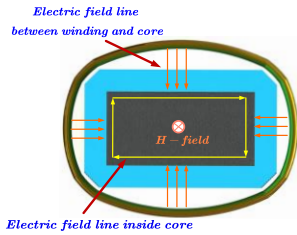


Fig. 4. Distribution of electric field lines in cross-section of a toroidal CM choke.

The general circuit model is depicted in Fig. 2. In this model, each turn is treated as an independent unit, comprising self-inductance (L_s) and core losses (R_s) in series, along with turn-to-turn capacitance (C_{tt}) in parallel. One end of the turn-to-core capacitance (C_{tc}) is connected to the left side of the unit, while the other end shares a common node with other C_{tc} . Since the last turn lacks an adjacent turn, the turn-to-turn capacitance between the first and second turns is divided into two equal parts. One part is in parallel with the last turn, with each part representing half of the turn-to-turn capacitance. As illustrated in Fig. 2, FEM is applied to reveal the distribution of electric field lines within a CM choke cross-section. It is obviously that

the electric field lines distributed in space between winding and core is perpendicular to and terminate at the surface of core, which is an equipotential surface, while rectangle closed electric field line distributing inside the core. However, these two sources of electric field lines are not the same. In space between winding and core, electric field lines terminate and perpendicular to the surface of the conductor, and the entire surface of the core can be treated as equipotential, as illustrated in Fig. 4. That is because perfect conductor assumption is commonly applied to CM chokes due to their high permeability and permittivity. As per this assumption, under the influence of a static electric field, charge is distributed over the surface of the conductor, resulting in a net electric field inside the conductor being zero. Meanwhile, inside the core, Faraday's law dictates that electric field lines are always perpendicular to the magnetic field, thereby forming a continuous closed curve to ensure tangential continuity at the boundary. The electric field lines run parallel to the boundary of the core cross-section, creating a rectangular closed curve. The two electric field lines don't intersect or interfere. Thus, that is the reason why C_c generated by the time-varying electric field can only be connected in parallel to the first and last turns of the winding from an energy perspective and C_{tc} have a common node, reflecting the equipotential surface. As a result, the impedance curve can be determined using circuit analysis methods at each frequency.

Upon the completion of the circuit model construction, the subsequent parameter extraction process is carried out. In traditional models, capacitance is often extracted using simplified geometries, resulting in significant errors in both capacitance and impedance curves, as will be demonstrated in Section III. Therefore, the consideration of the actual geometry, which includes complete insulation, winding bends, and helix lengths, is undertaken to improve the model's accuracy.

B. Complex Inductance Modeling

The complex relative permeability of the core is a crucial factor in inductance modeling, represented by its real part μ_r' , and its imaginary part μ_r'' . Consequently, the impedance (Z) of a single turn, when neglecting winding losses, can be expressed as follows:

$$Z = j\omega L_s + R_s \quad (1)$$

According to Ampère's circuital law, Z can be further expressed as follows:

$$Z = \mu_0 (\mu_r' - j\mu_r'') \frac{h_c}{2\pi} \ln\left(\frac{R_o}{R_{in}}\right) \quad (2)$$

Within CM chokes, the self-inductance of a single turn can

be denoted as L_{ii} , while the leakage inductance between turn i and turn j is represented as $L_{\sigma ij}$, and the mutual inductance between turn i and turn j is expressed as M_{ij} . The relationships among these parameters are as follows:

$$L_{ii} = M_{ij} + L_{\sigma ij} \quad (3)$$

In this paper, the neglect of leakage inductance is justified due to its orders of magnitude smaller magnitude compared to self-inductance.

C. Space Capacitance Modeling

In an effort to mitigate the detrimental impact of parasitic capacitance at HF, numerous studies have endeavored to precisely uncover its underlying mechanisms and develop models. Nonetheless, existing analytical models often encounter issues related to their applicability and lack of comprehensive consideration for various factors. For instance, questions arise regarding whether the model can be applied to single-layer chokes or if it accounts for actual electric field lines, the true geometry between turns and the core, insulations, and winding transitions. To achieve a more accurate model, contributions have been made by taking into account winding insulation, the actual turn-to-core distance, and the actual winding length.

As depicted in Fig. 3, C_{tt} and C_{tc} in different material regions can be analytically calculated using the following methods:

$$dC = \epsilon_0 dS / \sum_i (x_i / \epsilon_{ri}) \quad (4)$$

where dS represents the differential area, x denotes the electric lines path, ϵ_r is the relative permittivity of the medium. Building upon the theory presented in [8], in the calculation of parasitic capacitance, three distinct regions can be identified, which are outer region (C_{tto} , C_{tco}), inner region (C_{tin} , C_{tci}) and lateral region (C_{ttl} , C_{tcl}). However, it does not consider winding insulation. As shown in Fig. 2, the geometry between turns, turns, and the core is clearly illustrated. When accounting for winding insulation, both C_{tt} and C_{tc} can be re-expressed as follows:

$$C_{tt} = C_{tto} + C_{tin} + 2C_{ttl} \quad (5)$$

$$\left\{ \begin{aligned} C_{tto} &= \int_{-\pi/2}^{\pi/2} \frac{\epsilon_0 \epsilon_i \epsilon_a h_w (d_c/2 + w_i) \sin \alpha d\alpha}{2w_i \epsilon_a \sin \alpha + \alpha \epsilon_i [\delta_o + (d_c + 2w_i) (1 - \cos \alpha)]} \\ C_{tin} &= \int_{-\pi/2}^{\pi/2} \frac{\epsilon_0 \epsilon_i \epsilon_a h_w (d_c/2 + w_i) \sin \alpha d\alpha}{2w_i \epsilon_a \sin \alpha + \alpha \epsilon_i [\delta_{in} + (d_c + 2w_i) (1 - \cos \alpha)]} \\ C_{ttl} &= \int_{R_{in}}^{R_o} \int_{-\pi/2}^{\pi/2} \frac{\epsilon_0 \epsilon_i \epsilon_a (d_c/2 + w_i) \sin \alpha d\alpha}{\alpha \epsilon_i \left[\frac{\delta_o - \delta_{in}}{R_o - R_{in}} (r - R_{cin}) + (d_c + 2w_i) (1 - \cos \alpha) \right] + 2w_i \epsilon_a} \end{aligned} \right. \quad (6)$$

Equation (6) is explicit statement of equation (5). In these expressions.

$$C_{tc} = C_{tco} + C_{tci} + 2C_{tcl} \quad (7)$$

$$\left\{ \begin{aligned} C_{tco} &= \int_{-\pi/2}^{\pi/2} \frac{\epsilon_0 h_w (d_c/2 + w_i) \epsilon_a \epsilon_i \epsilon_{pl} \sin \alpha d\alpha}{\alpha \epsilon_i \epsilon_{pl} [w_{so} + (d_c/2 + w_i) (1 - \cos \alpha)] + \epsilon_a \sin \alpha (\epsilon_{pl} w_i + \epsilon_i w_{pl})} \\ C_{tci} &= \int_{-\pi/2}^{\pi/2} \frac{\epsilon_0 h_w (d_c/2 + w_i) \epsilon_a \epsilon_i \epsilon_{pl} \sin \alpha d\alpha}{\alpha \epsilon_i \epsilon_{pl} [w_{si} + (d_c/2 + w_i) (1 - \cos \alpha)] + \epsilon_a \sin \alpha (\epsilon_{pl} w_i + \epsilon_i w_{pl})} \\ C_{tcl} &= \int_{-\pi/2}^{\pi/2} \frac{\epsilon_0 (R_o - R_{in}) (d_c/2) \epsilon_a \epsilon_i \epsilon_{pl} \sin \alpha d\alpha}{\alpha \epsilon_i \epsilon_{pl} [w_{sl} + (d_c/2 + w_i) (1 - \cos \alpha)] + \epsilon_a \sin \alpha (\epsilon_{pl} w_i + \epsilon_i w_{pl})} \end{aligned} \right. \quad (8)$$

Equation (8) is explicit statement of equation (7). As depicted in Fig. 1 (b), because the conductor is not evenly fitted to the core, there is a need to adjust the distance between turns and the core. However, in traditional models, winding transitions are often overlooked. Therefore, in this paper, capacitive equivalence is employed, allowing for the derivation of an equivalent turn-to-core distance [11].

$$w'_s = 2\sqrt{w_c(w_c - w_e)} / \log \left(\frac{\sqrt{w_c} + \sqrt{w_c - w_e}}{\sqrt{w_c} - \sqrt{w_c - w_e}} \right) \quad (9)$$

Furthermore, in the traditional model, the coil length is typically assumed to be the perimeter of a rectangle. However, during the winding process, the coil length in the parallel region does not directly correspond to half of the difference between the inner and outer diameters of the inductor. Therefore, this paper incorporates corrections, as shown in Fig. 3 (c). The length of l'_w can be calculated using the cosine theorem.

$$l'_w{}^2 = 2R_{in}^2 (1 - \cos \varphi) + (R_o - R_{in})^2 - 2\sqrt{2(1 - \cos \varphi)} R_{in} (R_o - R_{in}) \cos((\pi + \varphi)/2) \quad (10)$$

The calculation of C_{tt} and C_{tc} using proposed general model, the traditional model presented in [8], and FEM simulations are illustrated in Fig. 5. The errors in dC_{tt} , dC_{tc} , C_{tt} , and C_{tc} obtained by the traditional model are 28.6%, 8.8%, 16.2%, and 26.2%, respectively. In contrast, the errors in the proposed general model are 8.3%, 0.1%, 2.4%, and 0.5%, respectively. These results unequivocally demonstrate the significantly higher accuracy achieved by the proposed model.

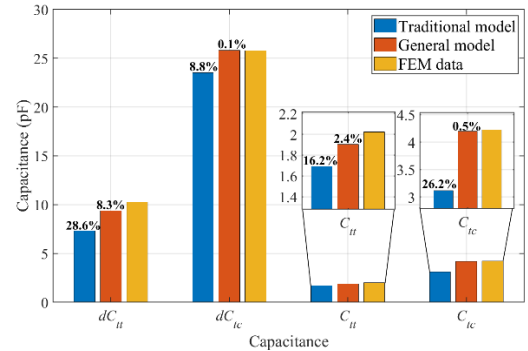


Fig. 5. Comparison among traditional model, proposed general model and FEM obtained space capacitance.

D. Core Capacitance Modeling

In accordance with the principles described in [12], an equivalent capacitance can be determined based on the energy associated with the time-varying electric field.

$$C_c = \epsilon_0 \epsilon_r l / 8 / \pi / N^2 \quad (11)$$

In this formula, ϵ_r represents the relative permittivity of the core, l is the equivalent circumference of the core, and N is the number of turns. This equation clarifies that C_c depends not only on the number of turns but also on the permittivity of core materials. Additionally, it's evident that the core capacitance is not influenced by the shape of the core's cross-section, making it applicable to CM chokes. However, it's important to note that the first resonant frequency, at which C_c becomes the dominant factor in the equivalent parasitic capacitance, may need adjustment due to the inductance associated with the cross-sectional shape of the core. Therefore, a formula for the first resonance point, denoted as f_R and tailored for rectangular cross-sections, is derived, which is suitable for widely used CM chokes.

$$f_R = \sqrt{1/L/C_{EPC}} / 2 / \pi = 2 / \sqrt{\mu_0 \mu_r \epsilon_0 \epsilon_r l h \ln(R_o/R_{in})} \quad (12)$$

Here, C_{EPC} signifies the total parasitic capacitance.

III. VERIFICATION AND DISCUSSION

Toroidal CM chokes with different numbers of turns, ranging from fewer turns to more turns tightly wound, have been manufactured, as depicted in the Fig. 6 and detailed in Table I. The testing equipment employed for these chokes is the WAYNE KERR 6500B impedance analyzer, covering a frequency range between 150kHz and 30MHz.

TABLE I
PARAMETERS OF TOROIDAL CM CHOKES [13-14]

Material	MnZn	Nanocrystal
Core permeability	$2 \times 10^3 \sim 1.5 \times 10^3$	$2 \times 10^4 \sim 2 \times 10^2$
Core permittivity	$2 \times 10^5 \sim 5 \times 10^4$	~ 10

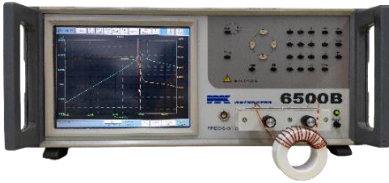


Fig. 6. Equipment and core used for experiments.

The testing results, as depicted in Fig. 7, clearly indicate that when examining CM chokes with 15 turns, the impedance curves generated by the proposed general model and the conventional model exhibit minimal discrepancies when compared to experimental data. However, the situation differs for chokes with 4 turns. In the case of 4-turn chokes, there is a 600 kHz difference in the resonance point frequencies between the impedance curves derived from the two methods. The proposed general model displays a 4% error when compared to the measured data, whereas the traditional model yields an error of 33%. When dealing with chokes containing 15 turns, the resonance frequencies between the impedance curves generated by the two methods differ by 50 kHz. The proposed general model displays a 3% error compared to the measured data, while the traditional model results in an error of 4.6%. In contrast, the general model consistently demonstrates significantly higher accuracy, particularly for CM chokes with a lower number of turns.

As depicted in Fig. 8, in order to assess the general applicability of the proposed model, tests were conducted on two cores made

from nanocrystalline materials. It is apparent that both the traditional model still exhibits significant errors when compared to the measured data and the general model, regardless of the number of turns considered. When dealing with chokes containing 6 turns, the error of our proposed general model in comparison to the measured data is 2.3%, whereas the traditional model yields an error of 45.1%. For chokes with 34 turns, the error of our proposed general model is 0.8%, while the traditional model results in an error of 25.3%. In these instances, significantly higher accuracy is consistently demonstrated by the proposed general model. Comparing these results with MnZn, it can be attributed to the fact that nanocrystalline materials possess low permittivity, resulting in minimal impedance impact. However, in this scenario, space capacitance plays a dominant role, leading to a significant error in the impedance curve, as illustrated in Fig. 8. It is feasible to recalibrate the space capacitance formula by considering the actual geometry.

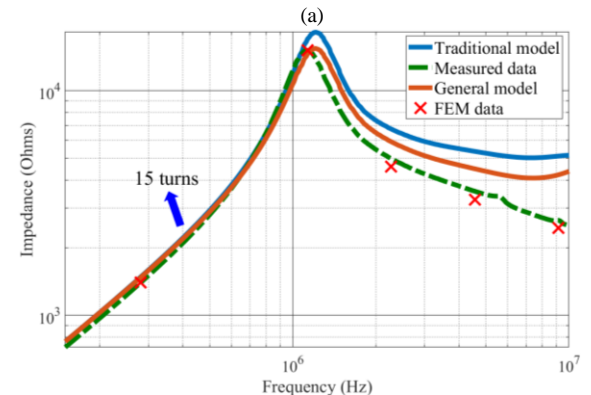
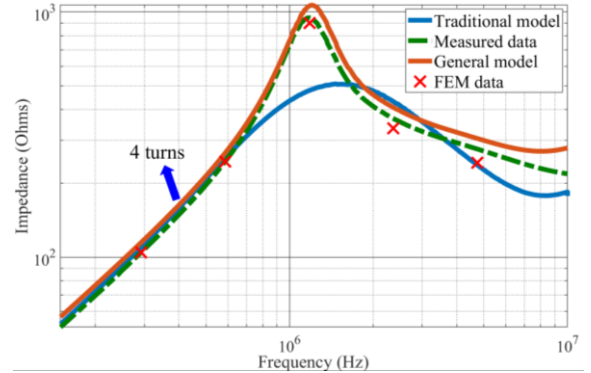


Fig. 7. Comparison among measured, traditional model, general model and FEM obtained impedance (MnZn). (a) 4 turns. (b) 15turns.

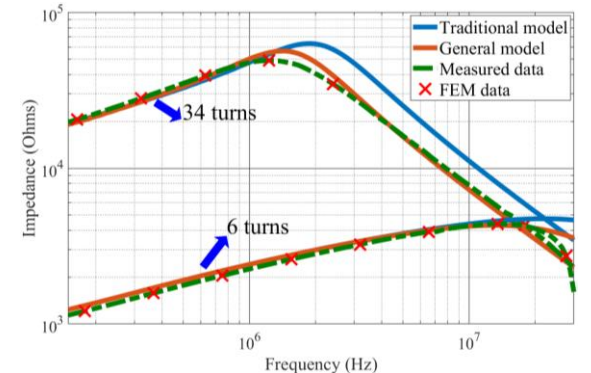


Fig. 8. Comparison among measured, traditional model, general model and FEM obtained impedance of CM chokes with 6 and 34 turns (Nanocrystal).

IV. CONCLUSION

This paper presents a comprehensive analytical model for single-layer CM chokes, aiming to overcome the limitations of traditional models and providing a detailed discussion of the model's physical significance. The proposed model addresses the influence of time-varying electromagnetic fields and integrates advanced techniques for deriving internal lumped parameters. To enhance accuracy, the model takes into account the actual geometric characteristics. Through simulation and experimental results involving various materials, the high modeling accuracy of the proposed general model for CM chokes with different geometries, core materials, and varying numbers of turns is convincingly demonstrated.

REFERENCES

- [1] Y. Zhang, Q. Li and D. Jiang, "A Motor CM Impedance Based Transformerless Active EMI Filter for DC-Side Common-Mode EMI Suppression in Motor Drive System," in *IEEE Transactions on Power Electronics*, vol. 35, no. 10, pp. 10238-10248, Oct. 2020.
- [2] Z. Shen et al., "Core Energy Capacitance of NiZn Inductors," in *IEEE Transactions on Power Electronics*, vol. 38, no. 4, pp. 4235-4240, April 2023.
- [3] Y. Li and S. Wang, "Modeling and Increasing the High-Frequency Impedance of Single-Layer Mn-Zn Ferrite toroidal Inductors With Electromagnetic Analysis," in *IEEE Transactions on Power Electronics*, vol. 36, no. 6, pp. 6943-6953, June 2021.
- [4] Á. Ojeda-Rodríguez, J. Bernal-Méndez and M. A. Martín-Prats, "Modal Theory and Approach for Accurate Characterization of Common-Mode Chokes," in *IEEE Transactions on Power Electronics*, vol. 38, no. 9, pp. 10516-10529, Sept. 2023.
- [5] X. Liu et al., "Behavioral Modeling of Complex Magnetic Permeability With High-Order Debye Model and Equivalent Circuits," in *IEEE Transactions on Electromagnetic Compatibility*, vol. 63, no. 3, pp. 730-738, June 2021.
- [6] N. Moonen, R. Vogt-Ardatjew, A. Roc'h and F. Leferink, "3-D Full-Wave High Frequency Common Mode Choke Modeling," in *IEEE Transactions on Electromagnetic Compatibility*, vol. 62, no. 3, pp. 707-714, June 2020.
- [7] H. Jie et al., "Characterization and Modeling of Single-Phase Common-Mode Chokes via Finite-Element Analysis," *IECON 2023- 49th Annual Conference of the IEEE Industrial Electronics Society*, Singapore, Singapore, 2023, pp. 1-6.
- [8] M. Kovacic, Z. Hanic, S. Stipetic, S. Krishnamurthy and D. Zarko, "Analytical Wideband Model of a Common-Mode Choke," in *IEEE Transactions on Power Electronics*, vol. 27, no. 7, pp. 3173-3185, July 2012.
- [9] S. Luan, Z. Yan and H. Zhao, "Effects of Airgaps on Parasitic Capacitance of Magnetic Components," in *IEEE Transactions on Power Electronics*, vol. 39, no. 1, pp. 1115-1134, Jan. 2024.
- [10] H. Zhao et al., "Physics-Based Modeling of Parasitic Capacitance in Medium-Voltage Filter Inductors," in *IEEE Transactions on Power Electronics*, vol. 36, no. 1, pp. 829-843, Jan. 2021.
- [11] F. Salomez, A. Videt and N. Idir, "Modeling and Minimization of the Parasitic Capacitances of Single-Layer toroidal Inductors," in *IEEE Transactions on Power Electronics*, vol. 37, no. 10, pp. 12426-12436, Oct. 2022.
- [12] R. Zhang, S. Wang, T. Long, J. Qiu, K. Liu and H. Zhao, "The Magnetized Capacitance, First Resonant Frequency, and Electromagnetic Analysis of Inductors With Ferrite Cores," in *IEEE Transactions on Industrial Electronics*.
- [13] Ferroxcube, "Data handbook," Tech. Rep., 2017. [Online]. Available: <https://www.ferroxcube.com/zh-CN/download/download/21>.
- [14] Vacuumschmelze, "Soft Magnetic Materials and Semi-finished Products," Tech. Rep., 2021. [Online]. Available: https://vacuumschmelze.com/03_Documents/Brochures/PHT%20001%20en.pdf.